

Rubric 2: SCIENTIFIC AND PRACTICAL DEVELOPMENTS

Field “Electrical Engineering”

DOI: 10.17816/transsyst20195216-30

© Weili Li, Zhigang Wu, Junci Cao, Dong Li
School of Electrical engineering, Beijing Jiaotong University
(Beijing, China)

STUDY ON HEAT EXCHANGE OF DIFFERENT VENTILATION STRUCTURES OF ASYNCHRONOUS TRACTION MOTOR FOR HIGH SPEED EMU

Background: Aiming at the problems of high local temperature and uneven temperature distribution in asynchronous traction motor of high-speed Electric Multiple Unit (EMU) when it is running.

Aim: In this paper, the influence of ventilation system with different structure on temperature distribution is studied.

Methods: Taking 600 kW asynchronous traction motor as an example, the electromagnetic-fluid-temperature analysis model of the traction motor is established, and the temperature values of different positions in the motor are obtained.

The accuracy of the calculation results is verified by comparing with the actual measurement.

On this basis, by adjusting the structure of stator and rotor axial ventilation holes, the relationship between temperature distribution and fluid flow state in motor is studied.

In addition, the influence of fluid incidence angle on fluid velocity and heat dissipation performance of motor is also studied, and the ventilation structure scheme with relative balance of axial and circumferential temperature in motor is found out, which provides a reference strategy for the design of temperature rise of motor with forced ventilation structure.

Results: The wind speed near the intake side of stator teeth and rotor teeth groove is less than that far from the intake side. The flow distribution trend of rotor vent is similar to that of stator vent, but the air in the groove is affected by centrifugal force of rotor rotation, which makes the wind speed difference on the intake side larger than that on the outlet side.

The stator winding and rotor guide bar are affected by wind temperature to reach the maximum temperature at the end of the outlet respectively. The stator core is higher at the windward side and the leeward side than the other parts of the motor. The heat dissipation effect at both ends is good.

The highest temperature of the stator core appears near the leeward side.

Key Words: Traction Motor, Ventilation System, Fluid Flow State.

© 李伟力, 吴志刚, 曹君慈, 李栋
北京交通大学电气学院
(中国北京)

高速动车组异步牵引电机不同通风结

摘要: 针对高速动车组异步牵引电机运行时局部温度高, 电机内温度分布不均匀的问题, 本文研究电机不同结构的通风系统对温度分布的影响. 以 600 Kw 异步牵引电动机为例, 建立了牵引电机电磁-流体-温度分析模型, 得到了电机内不同位置的温度值, 并与实测进行对比, 验证了计算结果的准确性. 在此基础上, 通过调整定子和转子轴向通风孔的结构形式, 研究电机内温度分布与流体流动状态的关系; 此外, 还研究流体入射角对流体流速与电机散热性能的影响, 找出电机内轴向及周向温度相对平衡的通风结构方案, 为强迫通风结构型式的电机温升设计提供参考策略.

关键词: 高速铁路牵引电机, 通风系统, 流体流动状态.

1. INTRODUCTION

The traction motor in the traction drive system is one of the core components of high-speed train and EMU. Its performance determines the quality of train power and is directly related to the safety of high-speed railway operation. Because of the limited space for motor placement in high-speed train, the high power density of motor and its large heat load, the motor heats seriously, which affects the service life of motor and the safety of train operation. At present, motor temperature control is the biggest bottleneck in the development of traction motor, the high ambient temperature makes the air intake temperature high; the air intake is blocked by debris, which makes the air intake not smooth, resulting in small air intake; the excessive dust inside the motor affects heat dissipation; the fan damage causes no wind or small air volume; the unreasonable ventilation structure makes the short circuit of the air circuit and so on will cause the motor to heat dissipation and increase temperature. If the motor works at the highest allowable temperature for a long time, it will accelerate insulation aging and eventually burn down the motor. Therefore, accurate calculation of the internal temperature of the motor is of great significance for improving the ventilation structure of the motor.

Many scholars have studied the fluid-structure coupling calculation of temperature-fluid. Dae G.K. establishes a three-dimensional coupling model of traction motor to solve the problem of heat dissipation caused by the closed structure of traction motor. The flow rate of cooling medium in the original model is analyzed. The cooling performance of traction motor is improved by changing its ventilation and cooling structure [1]. Mugglestone J. et al. used CFD software to simulate the flow field and heat transfer process in the stator end region of an air-cooled induction motor. The results show that the

circulating current is generated at the stator end winding side and the local heat transfer coefficient is estimated. The results show that the spatial variation of the fluid is correct [2]. Mayle E.R. et al. put forward an analysis method considering the rotating state of gas between stator and rotor of turbogenerator. This analysis also takes into account the changes of flow rate, angular momentum and static pressure in the incident region of cooling gas. Simple calculation shows that the average tangential velocity of this rotating gas flow is different from that of taking it as half of the rotating speed of the rotor. By comparison, the former is found to be more practical [3]. Xiaolong Lu analyzed the transient and steady-state temperature field of rotary ultrasonic motor by finite element method, and simulated the ultrasonic motor with different sizes. It was found that the temperature distribution of different types of motor had different inhomogeneity, and the time needed to achieve thermal stability was also different. However, the highest temperature point of the motor was located at the interface between the stator and the rotor, and passed through the simulation. Experiments verify the accuracy of the calculation method [4].

In this paper, the finite volume method in numerical algorithm is used to establish the three-dimensional global model of the motor. The air flow and temperature distribution in the motor are analyzed accurately by fluid-solid coupling, and the ventilation structure is improved accordingly.

2. ESTABLISHMENT OF MOTOR MODEL AND ANALYSIS OF FLUID COMPUTATION

2.1. Establishment of fluid-temperature model for traction motor

The traction motor of 600 kW high-speed train studied in this paper adopts axial ventilation cooling structure, and its basic rated parameters are shown in Table 1.

Table 1. Basic parameters of traction motor for high-speed train

Motor parameters	Value
Rated power/kW	600
Rated voltage/V	2730
Rated current/A	155
frequency/Hz	155.55
efficiency	94 %
Stator length/mm	270
Stator Dia/mm	555

In this paper, the motor adopts an open-circuit cooling axial ventilation mode, which is divided into three channels for ventilation, one way into the stator ventilation ditch, one way into the air gap between the stator and the rotor, one way into the rotor ventilation ditch. Fig. 1 is a schematic diagram of the ventilation structure of the motor. The direction indicated by the arrow is the direction of fluid flow in the motor.

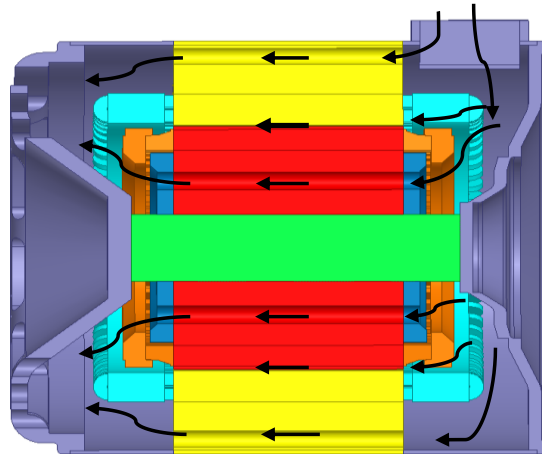


Fig. 1. Ventilation structure of traction motor for high-speed train

On this basis, in order to reasonably solve the fluid-structure coupling model of the motor, the basic assumptions are as follows.

(1) The Reynolds coefficient of air-fluid in the motor is larger than 2300, so there is turbulence in the motor, and the flow pattern of the fluid belongs to turbulence.

(2) Because of the small influence of buoyancy and gravity on the fluid flow in the motor under standard atmospheric pressure, it is neglected.

(3) The compressibility of gas is related to ambient temperature and external pressure. Whether the density change can be neglected depends on the Mach number of gas flow. Because the velocity of fluid flow in motor is less than that of sound, the fluid is treated as incompressible fluid [5].

(4) Winding insulation varnish uniformly.

(5) It is concluded that slot wedge and slot insulation are the same width and have the same insulation properties.

(6) In this paper, the steady flow state of fluid in the steady state of motor is studied, so the solving equation does not contain time variable [6].

(7) Assuming that the heat source density is evenly distributed in all parts of the motor [7].

The structure diagram of the motor is obtained as shown in Fig. 2.

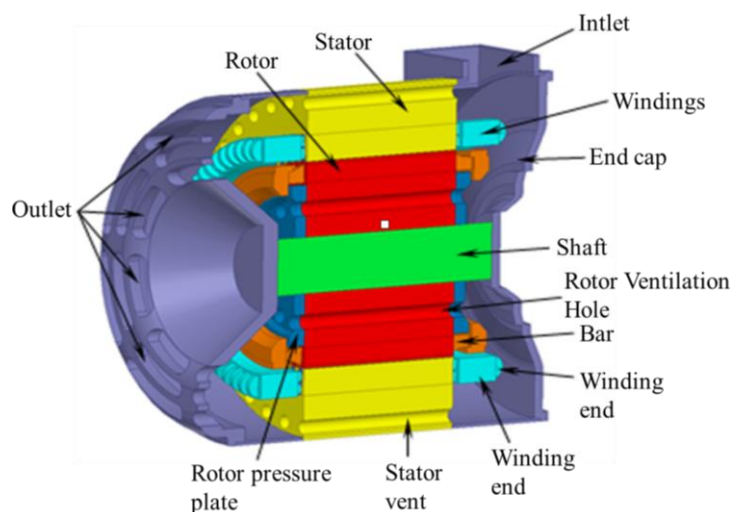


Fig. 2. Solving Domain Internal Structure Diagram

The loss of each part of the motor is obtained by the calculation and analysis of the electromagnetic field and the actual measurement results as shown in Table 2.

Table 2. Distribution Table of Motor Loss under Load

	Loss (kW)
Winding	5.814
Stator tooth	2.667
Stator yoke	5.825
Rotor guide bar	3.900
Additional loss	3.159

According to the characteristics of the solution domain, the following boundary conditions are listed.

(1) The entrance boundary condition is velocity entrance, and the entrance velocity is 25.5 m/s.

(2) The solid surfaces in contact with air are all set as non-slip boundary conditions.

(3) The air inside the rotor is a rotating flow field, and the stator air is simulated as a static state.

(4) The boundary condition of outlet is pressure outlet, and the initial pressure is one atmospheric pressure.

(5) According to the given losses, the heat sources of stator winding, stator yoke, stator teeth, rotor core and rotor guide bar are assigned respectively [8].

2.2. Analysis and experimental verification of calculation results of fluid-temperature field of traction motor

Fig. 3(a) shows the overall fluid flow state near the intake side, and Fig. 3(b) shows the overall fluid flow state far from the intake side. The flow vector diagram of the intake part is intercepted and enlarged, and the flow direction of the two parts above the intake and outlet cavity is analyzed respectively.

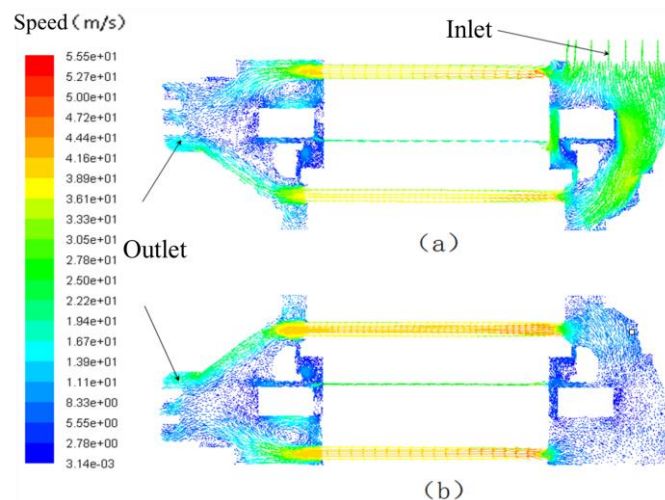


Fig. 3. Vector Chart of Fluid Velocity in Radial Section of Motor

The fluid trace of stator vent is shown in Fig. 4. It can be seen that the eddy current around the vent of stator vent is uniformly distributed in the bending part of stator winding end.

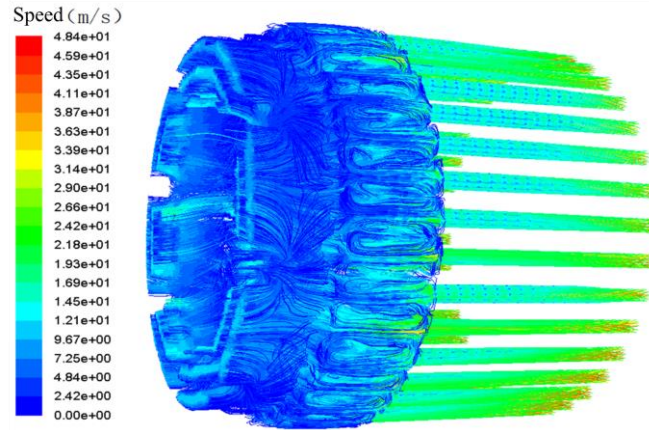


Fig. 4. Fluid Trace of Stator Ventilation Hole

According to the calculation of motor fluid, the temperature distribution of the motor is obtained. Fig. 5 shows the three-dimensional temperature distribution cloud of the whole motor. According to the results shown in the graph, the highest surface temperature of the stator core is about 117 °C. It appears near the outlet side of the axis center and transfers heat to the two ends of the shell. As the axial position moves toward the outlet, the closer the temperature is to the core part, the higher the temperature is. Because the fluid convection heat transfer between the core section and the heat source inside the motor, the overall air temperature at the outlet is higher than that at the inlet, which results in the temperature of the inlet casing being about 30 degrees lower than that of the outlet casing. The highest temperature in the motor is 217 °C, which appears on the end ring of the rotor in the air outlet chamber.

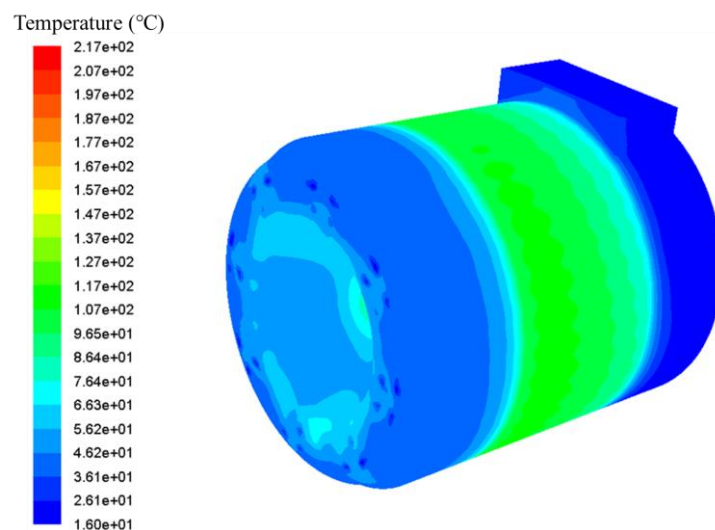


Fig. 5. Overall Temperature Distribution Cloud of Motor

In order to better study the internal temperature of the motor, the temperature of the central surface of the motor shaft is intercepted for analysis [9], as shown in Fig. 6. The temperature distribution of the stator winding is more uniform along the axis. The temperature distribution of the stator winding near the intake side is lower than that far away from the intake side. The temperature of the rotor guide bar is the highest in the whole section, and its temperature value is 159 °C. The heat transfer process of the stator part is that the stator winding is transferred to the slot insulation, and then to the given teeth and yoke of the stator. The heat transfer process of the rotor part is that the rotor guide bar is transferred to the core of the rotor, and then to the rotating shaft.

Under the rated condition of stable operation of the motor, the temperature at the yoke of the motor shaft center opposite the intake port near the root of the stator teeth was collected by embedding a temperature sensor. The temperature value was 110 °C, and the calculated value of the corresponding position was 111.92 °C.

At the same time, static and dynamic pressure experiments were carried out inside the intake. The results show that the measured static pressure is 1906 Pa, the calculated value of corresponding position is 1810 Pa, and the measured dynamic pressure is 727 Pa, and the calculated value of corresponding position is 697 Pa.

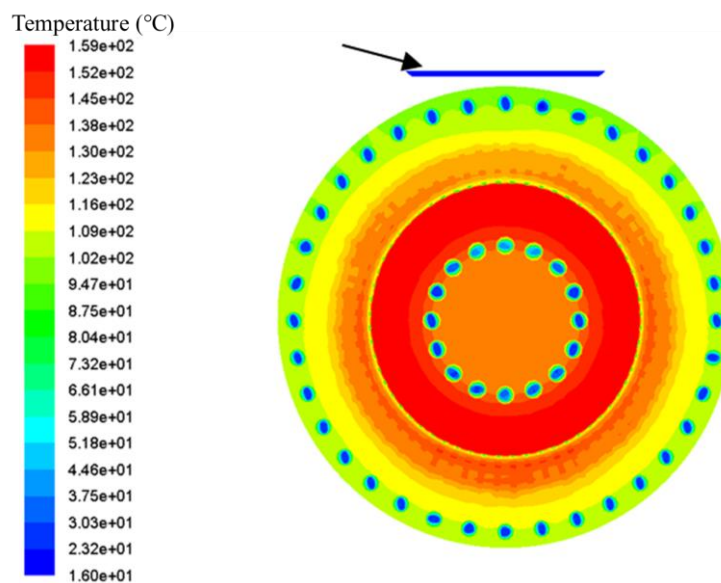


Fig. 6. Cloud Map of Temperature Distribution in the Center Section of Motor Shaft

By comparing the calculated and measured values of temperature, static pressure and dynamic pressure, it can be seen that the error between the calculated and experimental values of temperature is 1.7 %, the relative error of static pressure is 5.0 %, and the relative error of dynamic pressure is 4.1 %. The experimental results show that the model is consistent with the actual situation and the accuracy of the calculation method used.

3. FLUID AND TEMPERATURE FIELDS OF MOTORS WITH DIFFERENT VENTILATION STRUCTURES

Although the highest temperature occurs at the end ring of the rotor, the high temperature resistance of the rotor is strong, and the temperature rise of stator insulation is limited. In this paper, aiming at reducing the temperature rise of stator winding, the ventilation structure is improved, and the influence of the position of stator ventilation hole on the fluid and temperature field of the motor is studied. On the basis of this, the best scheme is selected. Then, the change of the inlet fluid incidence angle on the motor is studied. The influence of fluid field on internal temperature field.

3.1. Effect of Radial Position of Stator Ventilation Hole on Motor Fluid and Temperature

According to the fluid and temperature distribution characteristics of the original model, three schemes are proposed to adjust the radial position of the stator ventilation holes without changing the other structures of the motor, respectively, as shown in Fig. 7. The original model stator ventilation ditch is located at 0.2575 m of the core radial position. The three schemes set the ventilation holes at 0.247 m, 0.237 m and 0.227 m of the core radial position respectively.

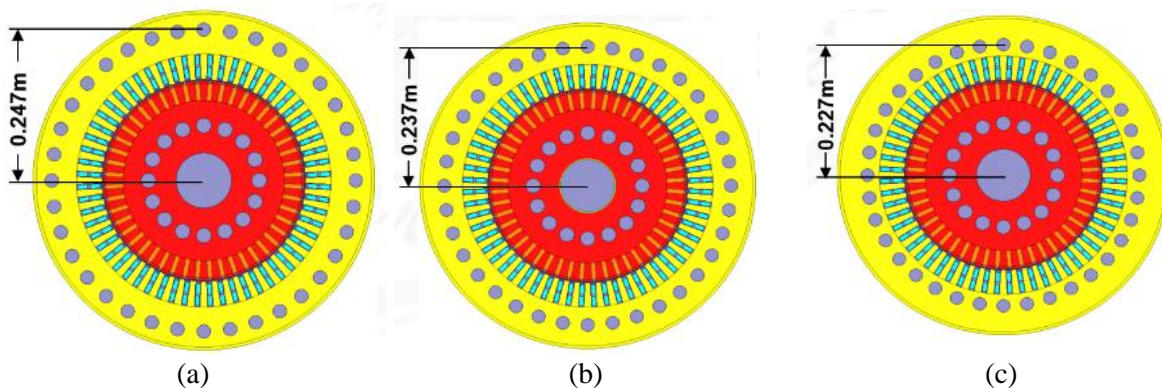
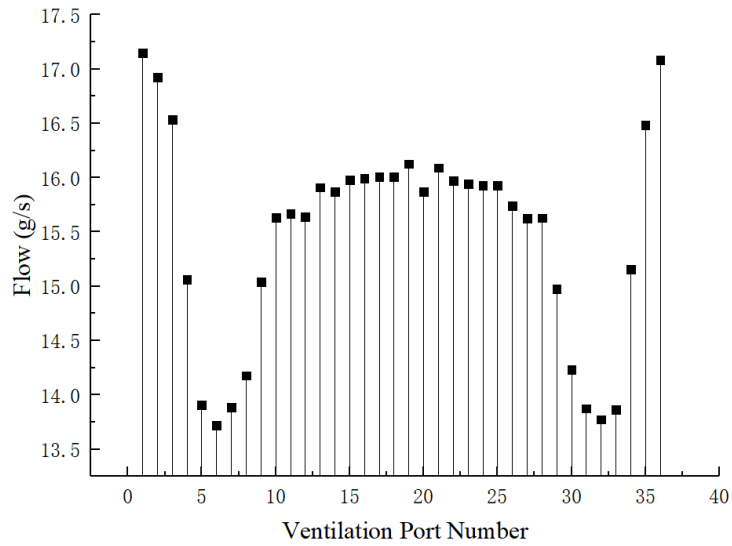
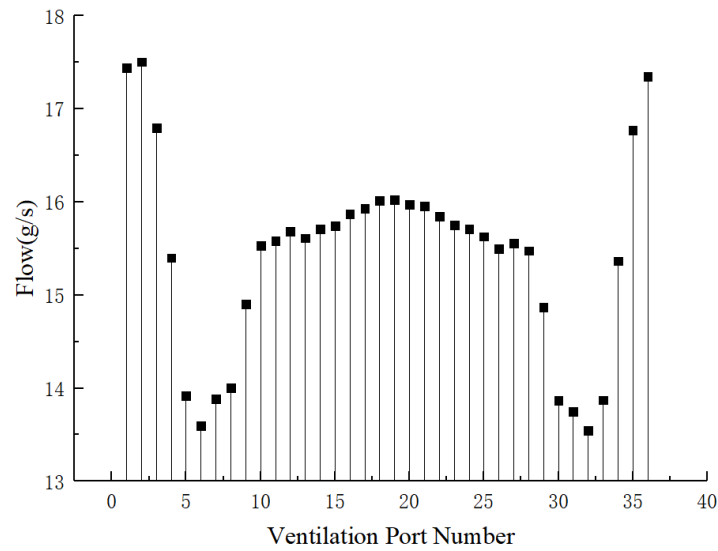


Fig. 7. Drawing of the position of ventilation holes in three schemes

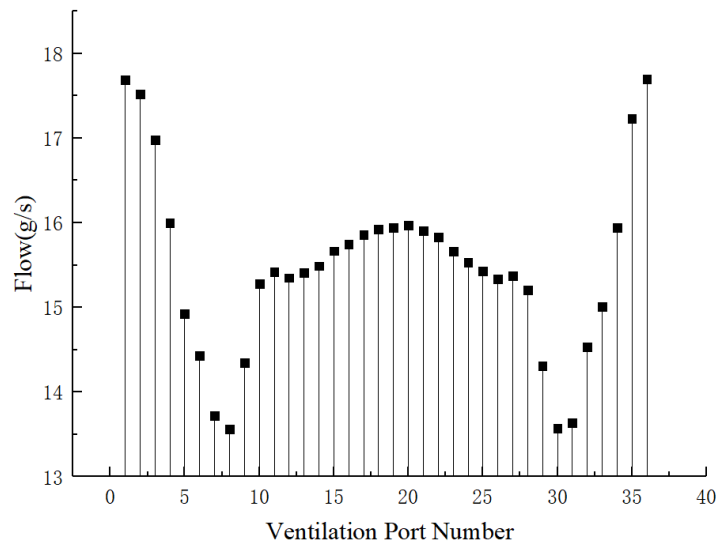
According to the order of the number of ventilation holes, the stator ventilation holes are named, and the flow rate at the entrance of each ventilation hole is intercepted for comparative analysis. Fig. 8 shows the flow distribution of each vent in three schemes.



(a) Scheme 1



(b) Scheme 2



(c) Scheme 3

Fig. 8. Circumferential Inlet Flow Distribution of Stator Ventilation Hole

The air flow distribution trends of the three schemes are basically the same. Unlike the original model, the flow distribution of the three schemes is positive to the intake and the flow near one side is larger than that far from the other side. Changing the position of the vent has no effect on the flow rate of the vent far from the intake side, but increases the flow rate near the intake side.

According to the temperature distribution of the stator winding of the original model, the stator winding with the highest temperature value is intercepted for analysis [10]. From the observation of Fig. 10, it can be seen that the three schemes have the same temperature rising trend and the same position of the highest point, all occurring at the axial length of 0.017 m. The highest temperature along the axis of the first scheme is 146 °C, the highest temperature in the second scheme is 143 °C, the highest temperature in the third scheme is 135 °C, and the highest temperature along the axis of the original model is 147 °C. It can be seen that the ventilation and heat dissipation effect of the three pairs of stator windings is relatively optimal, and the temperature of the highest temperature point is 12 °C less than that of the original model.

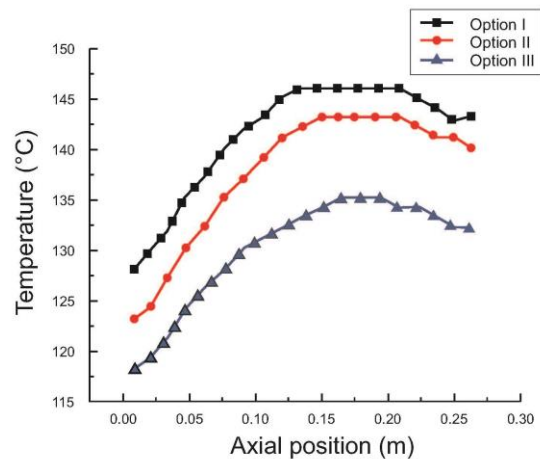
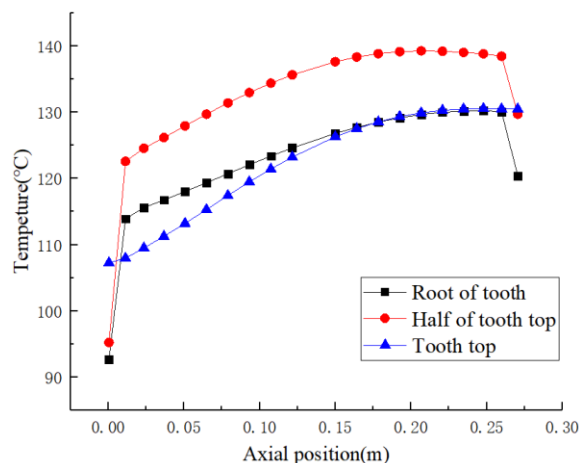
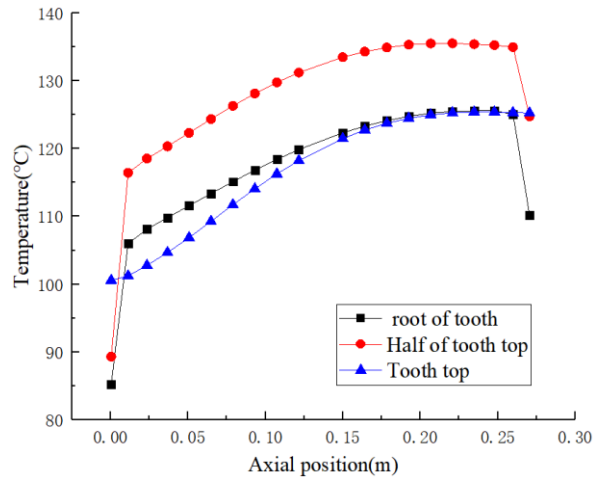


Fig. 9. Temperature profile of the stator winding along the axial direction

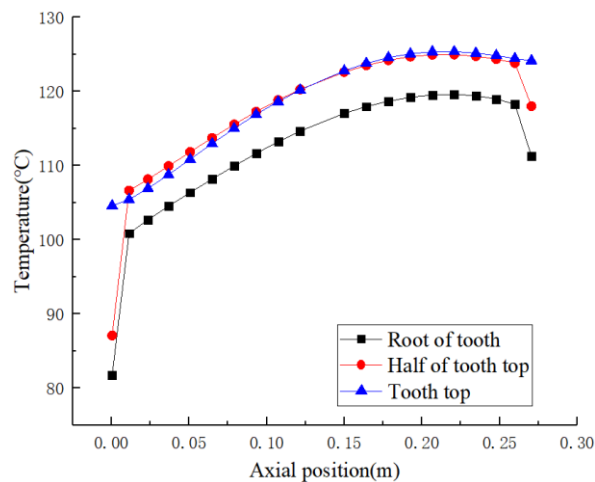
Select stator teeth that are facing air inlet and away from one side to analyze temperature change of tooth along axial direction.



(a) Scheme 1



(b) Scheme 2



(c) Scheme 3

Fig. 10. Temperature Change Diagram of Stator Tooth along Axis

The maps show that the change trend of tooth temperature of the three schemes is the same as that of the original model. The maximum temperature of the tooth top of the original model is 176.73 °C, the maximum temperature of the tooth top 1/2 is 182.76 °C, and the maximum temperature of the tooth root is 179.38 °C. In the first scheme, the maximum temperature of the top of the tooth is 130.57°C, the maximum temperature of the top 1/2 is 139.29 °C, and the maximum temperature of the root is 130.28°C. The maximum temperature of the second tooth top is 125.41°C, the maximum temperature of the top 1/2 is 135.52 °C, and the maximum temperature of the root is 125.59 °C. The maximum temperature at the top of the third tooth is 125.36 °C, 124.95 °C at the top 1/2 and 119.58 °C at the root of the third tooth.

3.2. Effect of different incident angles of fluid on fluid and temperature of motor

On the basis of the above, the influence of the inclined angle and direction of the intake port on the fluid and temperature field of the motor is studied, and a scheme is put forward [11].

Table 3. A Scheme of Changing the Inclination Angle of the Inclination Direction of the Inlet

Scheme	1	2	3	4
Inclination direction	stator	stator	cap	cap
Inclination angle	5°	10°	5°	10°

The nomenclature of stator ventilation holes is consistent with the basic model. According to the order of ventilation holes, the entrance flow of each ventilation hole is intercepted and analyzed separately, as shown in Fig. 11.

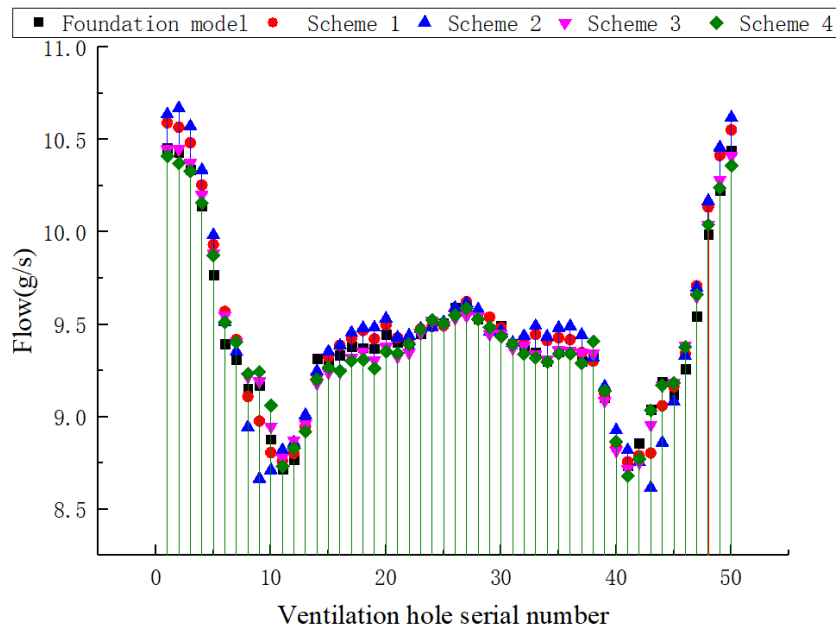


Fig. 11. Contrast Chart of Inlet Flow of Stator Ventilation Hole

From Fig. 11, it can be seen that changing the inclined direction and angle of the intake has little effect on the flow distribution of stator vents. The flow rate of the intake orifice is more than that of the basic model. The flow rate of the No. 1 vent is 0.14 g/s higher than that of the original model, but the flow rate of No. 8, No. 9, No. 10, No. 42 and No. 43 is lower than that of other schemes. The flow rate of No. 26 vent and other schemes is higher than that of the original model. Similarly, the flow rate near the No. 26 vent increased.

3.3. Contrastive Study on Temperature Field of Motor

Through fluid-solid coupling calculation, the temperature distribution inside the motor under each scheme is obtained.

Table 1. Temperature Distribution in Motor

°C	Winding	Stator yoke	Stator tooth	Slot insulation
Original	146.67	137.68	145.57	148.35
Scheme 1	128.07	119.42	126.7	129.38
Scheme 2	127.59	119.21	126.42	129.09
Scheme 3	125.52	118.34	125.24	127.7
Scheme 4	129.38	120.27	127.38	130.15

By comparing the stator windings of the above schemes, it can be seen that the stator winding temperature of scheme 3 is the lowest in all schemes, which is 4.73 °C lower than the basic model and 21.15 lower than the original model. The four schemes have the same temperature at the stator yoke and the tooth. The temperature value of the three yokes of the scheme is 2.02 °C lower than that of the basic model, and the temperature value of the tooth is 2.93 °C lower than that of the basic model. The insulation temperature of the observation tank shows that the temperature values of scheme 1 and scheme 2 are very close. The difference between scheme 4 and the basic model is very small. Scheme 3 has the lowest temperature, which is 3.27 °C lower than that of the basic model and 20.65 °C lower than that of the original model. The temperature of each scheme in the core part of the rotor is similar, of which scheme 4 has the lowest temperature and scheme 3 has the highest temperature, and its temperature value is close to the basic model. Therefore, from the angle of reducing the temperature rise of stator winding, the third scheme is the best choice.

4. CONCLUSION

The research work and results of this paper are as follows.

1) The wind speed near the intake side of stator teeth and rotor teeth groove is less than that far from the intake side. The flow distribution trend of rotor vent is similar to that of stator vent, but the air in the groove is affected by centrifugal force of rotor rotation, which makes the wind speed difference on the intake side larger than that on the outlet side.

2) The stator winding and rotor guide bar are affected by wind temperature to reach the maximum temperature at the end of the outlet respectively. The stator core is higher at the windward side and the leeward side than the other parts of the motor. The heat dissipation effect at both ends is good. The highest temperature of the stator core appears near the leeward side.

The authors make it expressly clear that:

1. No conflict of interests has taken or make take place;
2. The present article does not contain any researches with people involved as the objects of researches.

References / 参考

1. Kim DG, Kim SC. A Study on the Enhancement of the Cooling Structure for In-wheel Motor Transactions of the Korean Society of Automotive Engineers. *The Korean Society of Automotive Engineers*. 2013;21(1):36-42. doi: 10.7467/ksae.2013.21.1.036
2. Mugglestone J, Pickering S J, Lampard D. Prediction of the heat transfer from the end winding of a TEFC strip-wound induction motor [C]. IEEE International Electric Machines and Drives Conference. IEMDC'99. Proceedings (Cat. No.99EX272) 1999:671-681. doi: 10.1109/iemdc.1999.769153
3. Mayle RE, Hess S, Hirsch C, et al. Rotor-stator gap flow analysis and experiments [J]. *IEEE Transactions on Energy Conversion*. 1998;13(2):101-110. doi: 10.1109/60.678972
4. Lu X, Hu J, Zhao C. Analyses of the temperature field of traveling-wave rotary ultrasonic motors.[J]. *IEEE Transactions on Ultrasonics Ferroelectrics & Frequency Control*. 2011;58(12):2708-19. doi: 10.1109/tuffc.2011.2133
5. Valenzuela MA, Reyes P. Simple and reliable model for the thermal protection of variable speed self-ventilated induction motor drives [J]. *IEEE Transactions on Industry Applications*, 2010;46(2):770-778. doi: 10.1109/tia.2009.2039842
6. Mroz J. Temperature field of a double squirrel-cage motor during startup [J]. *IEEE Proceedings - Electric Power Applications*. 2005;152(6):1531-1538. doi: 10.1049/ip-epa:20045219
7. Cummings PG. Estimating Effect of System Harmonics on Losses and Temperature Rise of Squirrel-Cage Motors [J]. *IEEE Transactions on Industry Applications*. 1986;IA-22(6):1121-1126. doi: 10.1109/tia.1986.4504843
8. Bennion K, Cousineau J. Sensitivity analysis of traction drive motor cooling [C]. IEEE Transportation Electrification Conference and Expo (ITEC). 2012:1-6. doi: 10.1109/itec.2012.6243512
9. Mendes AMS, Lopez-Fernandez XM, Cardoso JM. Thermal evaluation of TEFC three-phase induction motors under different supply frequencies [C]. 18th International Conference on Electrical Machines. 2008:1-6. doi: 10.1109/icelmach.2008.4800075
10. Hruska K, Kindl V, Pechanek R, et al. Evaluation of different approaches of mathematical modelling of thermal phenomena applied to induction motors [C]. 2014 ELEKTRO IEEE. 2014:358-362. doi: 10.1109/elektro.2014.6848918
11. Nair DG, Jokinen T, Arkkio A. Coupled analytical and 3D numerical thermal analysis of a TEFC induction motor [C]. 18th International Conference on Electrical Machines and Systems (ICEMS). IEEE, 2015. doi: 10.1109/icems.2015.7385008

Information about the authors:

Weili Li, Doctor of Engineering Sciences, Professor;
ORCID: 0000-0003-4316-9642; Scopus Author ID: 8683345900;
E-mail: wlli@bjtu.edu.cn

Junci Cao, Doctor in Engineering, Associate professor;
ORCID: 0000-0003-1373-839X; Scopus Author ID: 35214365100;
E-mail: jccao@bjtu.edu.cn

Dong Li, Doctor in Engineering, Lecturer;
ORCID: 0000-0002-2359-9648; Scopus Author ID: 56610865300;
E-mail: donglz223624@126.com

Zhigang Wu, doctoral candidates;
ORCID: 0000-0003-1373-839X; Scopus Author ID: 57197774861;
E-mail: sdwuzhigang@163.com

有关作者的信息:

李伟力, 工学博士, 教授;
ORCID: 0000-0003-4316-9642; Scopus Author ID: 8683345900;
E-mail: wlli@bjtu.edu.cn

曹君慈, 工学博士, 副教授;
ORCID: 0000-0003-1373-839X; Scopus Author ID: 35214365100;
E-mail: jccao@bjtu.edu.cn

李栋, 工学博士, 讲师;
ORCID: 0000-0002-2359-9648; Scopus Author ID: 56610865300;
E-mail: donglz223624@126.com

吴志刚, 博士研究生;
ORCID: 0000-0003-1373-839X; Scopus Author ID: 57197774861;
E-mail: sdwuzhigang@163.com

To cite this article:

Li W, Wu Z, Cao J, Li D. Study on Heat Exchange of Different Ventilation Structures of Asynchronous Traction Motor for High Speed EMU. *Transportation Systems and Technology*. 2019;5(2): 16-30. doi: 10.17816/transsyst20195216-30

引用这篇文章:

李伟力, 曹君慈, 李栋, 李栋. 高速动车组异步牵引电机不同通风结构. *Transportation Systems and Technology*. 2019;5(2):16-30. doi: 10.17816/transsyst20195216-30